CENTRAL RESEARCH LIBRARY

ORNL-TM-4332

OAK RIDGE NATIONAL LABORATORY LIBRARIES
3 4456 0550194 4

cy.1

NEUTRAL BEAM INJECTION INTO A TOKAMAK I: FAST ION SPATIAL DISTRIBUTION FOR TANGENTIAL INJECTION

J. A. Rome
J. D. Callen
J. F. Clarke

OAK RIDGE NATIONAL LABORATORY
CENTRAL RESEARCH LIBRARY
DOCUMENT COLLECTION
LIBRARY LOAN COPY
DO NOT TRANSFER TO ANOTHER PERSON
If you wish someone else to see this document, send in name with document and the library will arrange a loan.
UCN-7969
(3 3-67)

OAK RIDGE NATIONAL LABORATORY
OPERATED BY UNION CARBIDE CORPORATION • FOR THE U.S. ATOMIC ENERGY COMMISSION

This report was prepared as an account of work sponsored by the United States Government. Neither the United States nor the United States Atomic Energy Commission, nor any of their employees, nor any of their contractors, subcontractors, or their employees, makes any warranty, express or implied, or assumes any legal liability or responsibility for the accuracy, completeness or usefulness of any information, apparatus, product or process disclosed, or represents that its use would not infringe privately owned rights.

ORNL-TM-4332

Contract No. W-7405-eng-26

Thermonuclear Division

NEUTRAL BEAM INJECTION INTO A TOKAMAK I: FAST ION SPATIAL DISTRIBUTION FOR TANGENTIAL INJECTION

J. A. Rome, J. D. Callen, and J. F. Clarke

[To be submitted for publication in Nuclear Fusion]

SEPTEMBER 1973

NOTICE This document contains information of a preliminary nature and was prepared primarily for internal use at the Oak Ridge National Laboratory. It is subject to revision or correction and therefore does not represent a final report.

OAK RIDGE NATIONAL LABORATORY
Oak Ridge, Tennessee 37830
operated by
UNION CARBIDE CORPORATION
for the
U.S. ATOMIC ENERGY COMMISSION

OAK RIDGE NATIONAL LABORATORY LIBRARIES

3 4456 0550194 4

NEUTRAL BEAM INJECTION INTO A TOKAMAK I:

FAST ION SPATIAL DISTRIBUTION FOR TANGENTIAL INJECTION*

J. A. Rome, J. D. Callen,† and J. F. Clarke

Oak Ridge National Laboratory, Oak Ridge, Tennessee 37830

ABSTRACT

The production processes and spatial distribution of fast ions resulting from tangential injection of a diffuse neutral beam into a tokamak are discussed. The spatial distribution of fast ions for various injection trajectories and absorption mean free paths are calculated and discussed in detail. Maximum beam absorption for a parabolic density profile is shown to occur for injection roughly halfway between the inner wall of the torus and the magnetic axis; however, since this maximum is near unity and only weakly dependent on the injection trajectory, this is not the most important possible optimization. Since the drift orbit surface area over which the fast ions are distributed is roughly proportional to the distance from the magnetic axis, the fast ion density is found to be strongly peaked at the magnetic axis for present experiments where the absorption mean free path λ is comparable to the plasma radius a. This geometric peaking effect is strong enough to overcome the exponential beam attenuation and cause the fast ion density and consequent beam energy deposition to be peaked at the plasma center as long as $\lambda_o \gtrsim a/4$. Charge

---

*Research sponsored by the U. S. Atomic Energy Commission under contract with the Union Carbide Corporation.

†On leave of absence from Massachusetts Institute of Technology.

exchange of the fast ions with neutrals in the plasma can deplete the fast ion population, particularly near the plasma edge. When charge exchange is an important loss mechanism, beam injection nearly tangent to the magnetic axis is found to maximize the beam effectiveness in heating.

NEUTRAL BEAM INJECTION INTO A TOKAMAK I: FAST ION SPATIAL DISTRIBUTION FOR TANGENTIAL INJECTION*

J. A. Rome, J. D. Callen,† and J. F. Clarke

Oak Ridge National Laboratory, Oak Ridge, Tennessee 37830

1. INTRODUCTION

The development of powerful neutral beam injectors [1] has made possible tokamak [2] experiments [3-6] in which the neutral power absorbed by the plasma can be comparable with the ohmic heating power and hence be expected to cause significant heating. Neutral beams also provide a particle source to offset the diffusion losses and can give rise to an electric current in the plasma [7,8]. The plasma current due to injection can supplement or decrease the ohmic current and/or act as a "seed" for the bootstrap current [9,10]. It may even be able to replace the transformer induced ohmic current and thereby allow operation of a steady state tokamak.

In addition to these desirable effects, neutral injection may have deleterious effects on plasma equilibrium and confinement in a tokamak. Plasma perturbations arising from neutral injection are caused primarily by the presence of a fast ion group and by the momentum imparted to the

---

*Research sponsored by the U. S. Atomic Energy Commission under contract with the Union Carbide Corporation.

†On leave of absence from Massachusetts Institute of Technology.

plasma by beam absorption. The various perturbations which occur, their interrelationships and possible limitations on this heating method will be discussed in a series of papers.‡

In this first paper we discuss the density and spatial distribution of the fast ions produced by tangential neutral beam injection, as in ORMAK. Injection roughly tangent to the magnetic axis (tangential injection) is generally preferred for the present experiments [3-5] because this leads to maximum beam absorption, minimum loss of the resulting fast ions to the limiter, and minimum trapping of the fast ions in any ripple of the toroidal B field. The geometry for tangential injection is illustrated in Fig. 1. The effects of beam divergence ($\sim 1.2^\circ$ in ORMAK) will be neglected in this work since they appear to have no qualitative effects on our results and their quantitative effects are very small. However, the finite size (or diffuseness) of the neutral beam is taken into account since it is important in determining the maximum fast ion density. The fact that the fast ions follow drift surfaces and not just flux surfaces, is a crucial ingredient in the analysis. In addition to being essential for estimating the magnitude of neutral beam induced plasma perturbations, the fast ion density distribution determines the spatial distribution of the neutral beam heating and hence is important for determining the effects of neutral beam heating in conjunction with plasma transport computer codes.

The paper is organized as follows. First, in Section 2 we briefly discuss the atomic processes which cause neutral beam absorption and give

---

‡When specific numbers are required in estimating the magnitudes of the various effects, we will use "standard" parameters for a single injector on the ORMAK experiment [3]. The standard (not best possible) ORMAK parameters used are listed in Appendix A.

rise to fast ions, with emphasis on the plasma perturbations produced by the absorption process. In the following section we discuss the absorption of a pencil beam and consequent spatial birth distribution of fast ions. Estimates of total beam absorption are also discussed in this section. Next, we assign the fast ions to the appropriate drift orbits and average over these orbits to obtain the fast ion density distribution for a pencil beam. Then, in Section 4 we average over a set of pencil beams representing the diffuse beam to obtain a fast ion density distribution. Section 5 deals with the effects of charge exchange between the fast ions and the cold neutrals in the plasma. Finally, in Section 6, we summarize our results.

2. ATOMIC PROCESSES

The dominant collision processes of energetic neutrals with tokamak-type plasmas are charge exchange, electron ionization, and proton ionization. Although it is not strictly correct for charge exchange, in this paper we will refer to these processes collectively as "ionization." The cross sections for these processes in the energy range of interest have been reviewed by Riviere [11], and conveniently summarized in Figs. 10 and 11 of Ref. [12]. For the standard ORMAK parameters (cf. Appendix A) the relevant cross sections and total mean free paths (at maximum plasma density) are tabulated in Table 1. Note that about 75% of the "ionizations" are by charge exchange collisions. Since only the relatively unimportant electron ionization cross section depends on the plasma temperature (and only weakly), the total "ionization" cross section is only very weakly dependent on the plasma temperature and this variation will be ignored. Hence the absorption mean free path is dependent only upon the local plasma density.

For each fast neutral "ionized" by the charge exchange process we produce a fast ion of essentially the same momentum as the incoming neutral and a "warm" neutral that has an energy on the order of the plasma ion temperature. The resultant source of "warm" neutrals for ORMAK appears to be about an order of magnitude below the natural source level in the plasma without injection and hence we will ignore it. [For reactor-type regimes this source may be quite significant near the magnetic axis and probably should be investigated in some detail.] The mean free path for reabsorption of these "warm" neutrals is about 10 - 15 cm and hence some of them may be reabsorbed within the ORMAK plasma.

For neutral breakup by impact ionization, in addition to the fast ion and the ionizing particle [whose energy is reduced by about the ionization energy ($\sim$ 15 eV)], we produce a "cold" electron which has an energy of approximately the ionization potential. The resultant electron is heated up to the plasma electron temperature in a very short time (typically $<$ 1 μsec) and hence is essentially indistinguishable from a background plasma electron. The energy required to heat these electrons up to the plasma electron temperature is negligible compared to the heat supplied to "cold" electrons produced by ionization of the neutrals which are in the plasma without injection and we will ignore it.

Thus, for each fast ion produced by absorption of a fast neutral, only $\sigma_{ion}/\sigma_T \sim 25\%$ (or perhaps a bit more if reabsorption of the "warm" neutrals is taken into account) are new, "extra" particles (an electron-ion pair) which can offset radial particle diffusion losses; the remaining $\sigma_{cx}/\sigma_T \sim 75\%$ of the ions are simply replacements of background ions by fast ions.

3. PENCIL BEAM CASE

In this section we consider a pencil beam with current I_B (in equivalent Amperes) that is injected in the plane $z = z_B$ and is tangent to the torus at $R = R_B$ as is shown in Figs. 1a and 1b. From the equation of the torus, we find that the beam enters (and leaves) the plasma at $R = R_o + \sqrt{a^2 - z_B^2}$. For simplicity, we assume that the beam does not intersect the inner side of the plasma torus at $R = R_o - \sqrt{a^2 - z_B^2}$.

3.1. BEAM ABSORPTION

If we define $I_B N_B(s)/e$ as the number of beam particles per second in a pencil beam at a point along the beam path, then the equation governing N_B is given by

$$\frac{dN_B}{ds} = -\frac{N_B}{\lambda(s)} \tag{1}$$

where $\lambda(s)$ is the mean free path of a neutral beam particle at point s. The general solution of this equation is

$$N_B(s) = N_B(-\infty)\exp[-D(s)] , \tag{2}$$

where the absorption decrement D(s) is given by

$$D(s) = \int_{-\infty}^{s} \frac{ds'}{\lambda(s')} , \tag{3}$$

and where $I_B N_B(-\infty)/e$ is the particle source rate of the pencil beam.

Since, as we have discussed in the preceeding section, the total absorption cross section is only very weakly dependent on the plasma properties, we can express the mean free path as

$$\lambda(s) = \frac{1}{n_e(s)\sigma_T} = \frac{n}{\lambda_o n_e(s)} \tag{4}$$

where $\lambda_o = 1/n\sigma_T$ is the absorption mean free path at the maximum plasma density, n.

In order to simplify the mathematics without losing any physical effects, we shall assume that the flux surfaces in the plasma are concentric circles. This is tantamount to assuming a large aspect ratio expansion and accordingly, to lowest order, that the flux surfaces are contours of constant plasma density. (The lowest order inverse aspect ratio correction causes the flux surfaces to nest slightly toward the outer edge of the torus [2].) Whenever we must use a density profile, we will assume a profile given by

$$n_e(r) = n\left[1 - \left(\frac{r}{a}\right)^2\right] . \tag{5}$$

Other profiles and corrections due to flux surface nesting can be easily used, but the physics does not change appreciably.

Using the facts that

$$r = [(R - R_o)^2 + z_B^2]^{1/2} , \tag{6}$$

$$ds = \mathrm{sgn}\,(s)\, RdR/(R^2 - R_B^2)^{1/2} , \tag{7}$$

and using the assumed parabolic density profile, we may write the absorption decrement in terms of the major radius, R:

$$D(s) = \frac{1}{\lambda_o} \left\{ - U(-s) \int_{R_o+\sqrt{a^2-z_B^2}}^{R} - U(s) \int_{R_o+\sqrt{a^2-z_B^2}}^{R_B} + U(s) \int_{R_B}^{R} \right\} \tag{8}$$

$$\times \, dR' \, \frac{R'[a^2 - (R' - R_o)^2 - z_B{}^2]}{a^2 \sqrt{R'^2 - R_B{}^2}} \, .$$

In this experssion, U is the unit step function defined by

$$U(s) = \begin{cases} 0 & s < 0 \\ 1/2 & s = 0 \\ 1 & s > 0 \, . \end{cases}$$

The integral in Eq. (8) can easily be shown to yield

$$F(R) = \int \frac{R'[a^2 - (R' - R_o)^2 - z_B{}^2]}{a^2 \sqrt{R'^2 - R_B{}^2}} \, dR' \tag{9}$$

$$= \frac{\sqrt{R^2-R_B{}^2}}{a^2} [a^2-z_B{}^2-R_o{}^2+R_oR - \frac{2}{3} R_B{}^2 - \frac{1}{3} R^2] + \frac{R_oR_B{}^2}{a^2} \ln [R + \sqrt{R^2-R_B{}^2}] \, .$$

Since the inverse aspect ratio a/R_o is small and since we expect R, R_B, and R_o to differ by no more than a, many parts of F(R) nearly cancel each other.

It is sometimes convenient to expand F(R) in the smallness of a/R, $\delta R/R_o$, and $\delta R_B/R_o$ where

$$\delta R \equiv R - R_o \; ; \quad \delta R_B \equiv R_o - R_B \, .$$

Then, making use of the relation

$$\ln\left(\frac{x^2 + \sqrt{x^2 - A^2}}{A}\right) = \sinh^{-1}\left(\frac{1}{A}\sqrt{x^2 - A^2}\right)\,\mathrm{sgn}(x)\ ,$$

and expanding $\sinh^{-1}$ to fifth order in its argument, we obtain

$$F(R) \simeq \sqrt{2R_o(\delta R+\delta R_B)}\ \left[\ 1 - \left(\frac{z_B}{a}\right)^2 - \frac{1}{5}\left(\frac{\delta R}{a}\right)^2 - \frac{8}{15}\left(\frac{\delta R_B}{a}\right)^2 + \frac{4}{15}\frac{\delta R\delta R_B}{a^2}\ \right] + \frac{R_o R_B^{\,2}}{a^2}\ln\left(\frac{R_B}{a}\right)\ . \tag{10}$$

In terms of F(R), the damping decrement can be written as

$$D(s) = \frac{1}{\lambda_o}\left\{\ U(-s)\ \left[\ F\left(R_o + \sqrt{a^2 - z_B^{\,2}}\right) - F(R)\ \right] + U(s)\ \left[\ F\left(R_o + \sqrt{a^2 - z_B^{\,2}}\right) - 2F(R_B) + F(R)\ \right]\right\}\ . \tag{11}$$

The total beam absorption in the equatorial plane is given by

$$D(\infty) = \frac{2}{\lambda_o}\left\{\ F(R_o + a) - F(R_B)\ \right\} \simeq \frac{2a}{\lambda_o}\sqrt{\frac{2R_o}{a}\left(1 + \frac{\delta R_B}{a}\right)}\ \left[\ \frac{4}{5} - \frac{8}{15}\left(\frac{\delta R_B}{a}\right)^2 + \frac{4}{15}\frac{\delta R_B}{a}\ \right]\ . \tag{12}$$

Maximizing this with respect to δR_B, we find that the maximum beam absorption occurs for

$$R_{B_{opt}} = R_o - \frac{a}{2} \tag{13}$$

(i.e. halfway between the magnetic axis and the inner edge of the plasma) and corresponds to a maximum damping decrement of

$$D_{max}(\infty) \simeq \frac{8a}{5\lambda_o}\sqrt{\frac{3R_o}{a}}\ . \tag{14}$$

For the typical ORMAK parameters in Appendix A, this corresponds to beam absorptions of 93, 97, and 99% for the 25, 25/2, and 25/3 keV beam components, respectively.

It is important to note that the beam absorption is not a very sensitive function of R_B. For instance, if $R_B = R_o$ (injection tangent to the magnetic axis), then $D(\infty)$ is decreased by only a factor of $\sqrt{3/2} \simeq 1.22$. Deviations of the density profile from the assumed parabolic shape will obviously change the beam path for optimum absorption. If, for instance, we assume a flat density profile, we maximize the beam absorption by maximizing the path length in the plasma, namely $R_B = R_o - a$. Conversely, as the density profile becomes more peaked on the magnetic axis, the optimum R_B approaches R_o. However, since the beam absorption is nearly total anyway, maximum beam absorption may not be the most appropriate optimization criterion.

In summary, beam absorption is estimated to be quite large (> 90%) and not critically dependent on the precise beam trajectory or density profile.

3.2. FAST ION BIRTH DISTRIBUTION

Since the rate of fast ion production per unit major radius, $(I_B/e)(dN_f/dR)$, is just the negative of the rate of beam loss per unit major radius, we have

$$\frac{dN_f}{dR} = -\frac{dN_B}{dR} = -\frac{dN_B}{ds}\frac{ds}{dR}$$

$$= \frac{1}{\lambda_o}\frac{[a^2-(R-R_o)^2-z_B{}^2]}{a^2}\frac{R}{\sqrt{R^2-R_B{}^2}}\{\exp\frac{1}{\lambda_o}[F(R_o+\sqrt{a^2-z_B{}^2})-F(R)]$$

$$+\exp\frac{1}{\lambda_o}[F(R_o+\sqrt{a^2-z_B{}^2})-2F(R_B)+F(R)]\}U(R-R_B)\ . \qquad (15)$$

In obtaining this expression, we have used the fact that s(R) is bi-valued, and we have added the two terms together which pertain for a given value of R. In addition, we have used the relation $N_B(-\infty) = I_B/e$ where I_B is the beam current in equivalent amperes. The singularity at $R = R_B$ is, of course, due to the fact that the beam is tangent to the torus at this point.

A plot of $\lambda_o\ dN_f/dR$ appears in Fig. 2 for $R_B = R_{B_{opt}}$ and $z_B = 0$ in ORMAK, with a/λ_o as a parameter. It is seen that: (1) dN_f/dR goes to zero linearly at the plasma edge due to the fact that the plasma density goes to zero there; (2) for small mean free paths relative to the plasma radius, after passing through the low density region, dN_f/dR decays exponentially as the beam proceed into the plasma; (3) the singularity due to the beam tangency occurs at $R = R_B$ if any particles manage to reach this far into the plasma; and (4) significant amounts of the beam reach the magnetic axis even for λ_o as small as a/4.

3.3. FAST ION DENSITY DISTRIBUTION

Once the fast ions are born at given points in the plasma, they are acted upon by the equilibrium electromagnetic fields in the plasma. Since the average time for collision of the fast ion with the background plasma ($\sim$ 10 msec)

is much greater than the time it takes for the ion to circumnavigate the torus ($\sim$ 10 μsec), it is appropriate to examine the single particle orbits for constant particle energy and magnetic moment.

The ion orbits are composed of a fast gyromotion about the magnetic field and a guiding center drift. The guiding center motion has been discussed in detail by Northrop [13] and specific orbits for fast ions in a tokamak have been derived by Stix [14]. In this paper, we only note the following points:

The pitch angle of the fast ion is determined by the beam geometry and point of ionization. For $R_B > \sqrt{(R_o+a)(2a)}$ ($\sim$ 68.7 cm in ORMAK), no injected ions will be trapped by the 1/R variation of the toroidal magnetic field. We will ignore trapped particles in this work since they occur, if at all, only at the edge of the plasma where the ion production rate is low and where they may be lost to the limiter.

The guiding center motion of an untrapped ion is determined by its motion along the magnetic field and by its $\underline{\nabla B}$ and curvature drifts. Near the magnetic axis, and in the equatorial plane, the z component of the guiding center velocity along the magnetic field, $v_{\parallel}$, can be exactly balanced out by the z component of the drifts and hence an ion born at this point (the stagnation point) will only move toroidally. For $v_{\parallel} >> v_{\perp}$, this point is located x_s away from the magnetic axis where

$$x_s \simeq \frac{qv}{2\Omega} \left[\frac{1 + \cos^2(v_{\parallel}/v)}{\cos(v_{\parallel}/v)} \right] \operatorname{sgn} (\underline{v} \cdot \underline{J}_{\text{plasma}}) , \tag{16}$$

q is the "safety factor," and Ω is the cyclotron frequency. We will refer to injection in the direction of the plasma ohmic-heating current, $\underline{v} \cdot \underline{J} > 0$, as coinjection, and conversely to the case of $\underline{v} \cdot \underline{J} < 0$ as counterinjection.

To lowest order in inverse aspect ratio, ions born away from the stagnation point have drift orbits which are concentric with the stagnation point provided that $q(r) \simeq$ constant, which is true near the center of the plasma. Allowing q to vary with r would shift the center of each orbit and appreciably increase mathematical difficulties without changing the physics involved.

If we define the distance from the stagnation point as ρ (see Fig. 1b), then the ions born at a point on the beam path will spread themselves roughly uniformly [15] over a ρ = constant surface of area $4\pi^2 R_o \rho$. This density will be roughly uniform in the poloidal direction since we assume $v_{\parallel} >> v_{\perp}$, and as we shall explicitly show in a later paper in this series [15], the ions will spread toroidally due to toroidal drift if they complete many guiding center orbits before they collide with the background plasma. Thus, the density of fast ions born on a given drift surface (ρ = constant) is given by

$$\dot{n}_f(\rho) = \frac{I_B}{4\pi^2 R_o \rho e} \frac{dN_f}{dR} \left| \frac{dR}{d\rho} \right| . \tag{17}$$

Since

$$R = R_o + x_s \pm \sqrt{\rho^2 - z_B^2} ,$$

the population on a given drift surface may have contributions from two values of R. Thus, we write

$$\dot{n}_f(\rho) = \frac{I_B/e}{4\pi^2 R_o \sqrt{\rho^2 - z_B^2}} \left\{ \left. \frac{dN_f}{dR} \right|_{R = R_o + x_s + \sqrt{\rho^2 - z_B^2}} + \left. \frac{dN_f}{dR} \right|_{R = R_o + x_s - \sqrt{\rho^2 - z_B}} \right\} U(\rho - z_B) . \tag{18}$$

The $U(\rho-z_B)$ arises because a beam at z_B can only populate drift surfaces with $\rho > z_B$, and the square root singularity arises from $|dR/d\rho|$. It should be noted that for a pencil beam in the equatorial plane, $\dot{n}_f(\rho)$ is singular at $\rho = 0$ like $1/\rho$ because the volume of the drift surface of a particle born on the stagnation point goes to zero. In addition, for $z_B \neq 0$, there is a milder singularity due to $dR/d\rho$ becoming infinite.

Figure 3 shows $\dot{n}_f(\rho)$ for $R_B = 68.5$ cm in ORMAK and for $a/\lambda_o = 1/2$. The singularities at $\rho = R_o - R_B$ and $\rho = 0$ are both evident here. As we shall see in the next section, however, all of these singular features are eliminated when we consider the effects of finite beam width.

4. A DIFFUSE BEAM

The actual beam used for neutral injection has a finite beam radius, r_B ($\sim$ 6 cm in ORMAK) and a given current density distribution over its cross section, $J(R_B,z_B)$, where $\iint_{\text{Beam}} J(R_B,z_B)dR_B dz_B = I_B$. In the present subsection we will integrate the pencil beam results of the preceding subsection over this diffuse beam cross section.

4.1. FAST ION DENSITY

It is convenient to normalize the fast ion density in the following manner:

$$\dot{n}_f(r,\Theta) = \frac{I_B}{e(2\pi R_o)(\pi a^2)} H(r,\Theta) , \tag{19}$$

where $H(r,\Theta)$ is a shape factor which, when integrated over the plasma volume, and divided by the volume yields the percentage of the fast ions

which are contained in the plasma. To lowest order in inverse aspect ratio,

$$\frac{1}{\pi a^2}\int_0^a\int_0^{2\pi} H(r,\Theta)r\,d\Theta\,dr = \%\text{ of fast ions contained in plasma.} \quad (20)$$

As the fast ions slow down, they remain reasonably close (namely, within a distance $\sim x_s$) to their birth flux surface. Thus, if we ignore charge exchange losses, the density profile of the fast ions is quite similar to the $\dot{n}_f$ profile and will grow linearly with time until the density reaches a quasi-steady state (at $n_f \sim 10^{12}/cm^3$ for the standard ORMAK parameters) at about one slowing down time (10 - 20 msec). The effect of charge exchange losses will be discussed in Section 5.

We now integrate the fast ion density input rate for a pencil beam, Eq. (19), over the finite beam size, i.e. over R_B and z_B. The limits require careful treatment. For fixed z_B, the R_B integration will run from the inner beam edge at $R_B = R_c - \sqrt{r_B^2 - z_B^2}$ to the outer beam edge at $R_B = R_c + \sqrt{r_B^2 - z_B^2}$ or to $R_B = R$, whichever is smaller. This occurs because of the step function in $d\dot{N}_f/dR$ and is physically due to the fact that the beam cannot populate a value of R which it does not reach. Then, using symmetry, the z_B integral runs from zero to the minimum of ρ or r_B in accord with the step function in Eq. (19). Thus,

$$H(\rho) = \frac{a^2}{I_B} \int_0^{\min\{\rho, r_B\}} \frac{dz_B}{\sqrt{\rho^2 - z_B^2}} \left[\int_{R_c - \sqrt{r_B^2 - z_B^2}}^{\min\{R_o + x_s + \sqrt{\rho^2 - z_B^2},\ R_c + \sqrt{r_B^2 - z_B^2}\}} J \frac{dN_f}{dR} \Bigg|_{R = R_o + x_s + \sqrt{\rho^2 - z_B^2}} dR_B \right.$$

$$\left. + \int_{R_c - \sqrt{r_B^2 - z_B^2}}^{\min\{R_o + x_s - \sqrt{\rho^2 - z_B^2},\ R_c + \sqrt{r_B^2 - z_B^2}\}} J \frac{dN_f}{dR} \Bigg|_{R = R_o + x_s - \sqrt{\rho^2 - z_B^2}} dR_B \right], \tag{21}$$

and,

$$H(r,\theta) = H(\rho) \Bigg|_{\rho = \sqrt{r^2 + x_s^2 - 2r\, x_s \cos\theta}} . \tag{22}$$

Since the beam current profile is reasonably uniform, we will henceforth assume that it is given by $J = I_B/\pi r_B^{\ 2}$.

In practice, it is easier to do the R_B integral before substituting for R. The loss of injected ions to the limiter is taken into account by only allowing $0 \leq \rho \leq a - x_s$; this is equivalent to saying that the ions born in the innermost (outermost) $2x_s$ of the plasma are lost to the limiter for coinjection (counterinjection).

It is important to note that since z_B is constrained to be $\leq \rho$, for small values of ρ and z_B, the integrand is non-singular, except for the $\sqrt{\rho^2 - z_B^{\ 2}}$ in the denominator, and in fact approaches a value $C/\sqrt{\rho^2 - z_B^{\ 2}}$ where C is a constant. Thus for small values of ρ, the integral will approach $C\pi/2$ and hence the stagnation point singularity will disappear. Physically, this is due to the fact that, for a diffuse beam, only an infinitesimal number of particles can be born on the stagnation point. In addition, since R_B can never be zero, the singularity at $R = R_B$ is integrable and hence there are no singularities in $H(r,\Theta)$.

4.2. CALCULATION OF $H(\rho)$

$H(\rho)$ is given by the complicated expression, Eq. (21). Although it can be evaluated numerically, a good idea of the shape of $H(\rho)$ can be obtained from merely studying the expression.

In general, $H(\rho = a - x_s)$ will be non-zero but small due to the low density at the edge of the plasma. A finite contribution to it will occur only if the beam passes through the circle $\rho = a - x_s$ at the value of R which is away from the stagnation point (i.e., $R = R_o + a - 2|x_x|$ for counterinjection and $R = R_o - a + 2|x_s|$ for coinjection).

For $\rho > r_B$, the upper limit on the z_B integral is fixed at r_B. If we ignore the ρ variation of dN_f/dR, (i.e. the beam attenuation) $H(\rho)$ will go as $\sin^{-1}(r_B/\rho) \sim 1/\rho$, provided we stay away from the low density region near $r = a$. In the region $\rho < r_B$, $H(\rho)$ will be approximately constant since the integrand of the z_B integral goes as $1/\rho$ while the upper limit goes as ρ.

The particular value $H(\rho = 0)$ can be estimated fairly accurately and is very useful in determining how the hot ions heat the center of the plasma. To make this estimate, we assume that the beam tangency point is well inside the magnetic axis, i.e. $R_o - R_c \gg r_B$. Accordingly, we neglect the contribution to the birth density at the stagnation point arising from the outward going half of the beam trajectory since it is exponentially small compared to the density arising from the inward going half. Since r_B is small, we set $z_B = 0$ in comparison to terms of order a.

If we define

$$\mathcal{f}(R) = F(R_o + a) - F(R) , \tag{23}$$

then, from Eq. 15,

$$\frac{dN_f}{dR} \simeq \frac{R_o}{\lambda_o} \frac{e^{-\frac{a}{\lambda_o}\mathcal{f}(R_o + x_s)}}{R^2 - R_B^{\,2}} , \tag{24}$$

where we have set $R = R_o + x_s$ everywhere except in the square-root singularity and we have ignored x_s and r_B compared to a. From Eq. (21), we obtain

$$H(\rho) \simeq \frac{a^2}{\pi r_B^{\,2}} \frac{R_o}{\lambda_o} \int_0^{\min\{\rho,\, r_B\}} \frac{dz_B}{\sqrt{\rho^2 - z_B^{\,2}}} \left\{ \int_{R_c - r_B}^{\min\{R_o + x_s,\, R_c + r_B\}} \frac{dR_B}{\sqrt{R^2 - R_B^{\,2}}}\, e^{-\frac{a}{\lambda_o}\mathcal{f}} \right\} \Bigg|_{R \,\pm\, R_o + x_s \,\pm\, \sqrt{\rho^2 - z_B^2}} . \tag{25}$$

Both signs must be used in switching variables from R to ρ and the results must be added.

Setting $R_B \simeq R_c$ in $\mathcal{f}$, the R_B integral yields

$$H(\rho) \simeq \frac{2R_o a^2}{\pi r_B^{\,2} \lambda_o} \int_0^{\min\{\rho,\, r_B\}} \frac{dz_B}{\sqrt{\rho^2 - z_B^2}}\, e^{-\frac{a}{\lambda_o}\mathcal{f}} \left[\sin^{-1}\left(\frac{R_c + r_B}{R_o}\right) - \sin^{-1}\left(\frac{R_c - r_B}{R_o}\right)\right] .$$

The factor of 2 is due to the fact that we set $R \simeq R_o$ for both signs when switching variables. For ρ very small (but greater than z_B) the z_B integral yields $\pi/2$. Furthermore, we may expand the $\sin^{-1}$ terms about the point where their argument is unity and assume $r_B \ll \delta R_c$ where $\delta R_c \equiv R_o - R_c$. Thus, we finally obtain

$$H(\rho \simeq 0) \simeq \frac{a^2}{\lambda_o r_B} \sqrt{\frac{2R_o}{\delta R_c}}\, e^{-\frac{a}{\lambda_o}\delta} . \tag{27}$$

Since $H(\rho)$ is in general approximately constant for $\rho \lesssim r_B$ and then falls off as $1/\rho$, if $r_B > x_s$, $H(\rho = 0) \simeq H(r = 0)$ and hence, the flux surface average, $\langle H(r,\theta)\rangle_\theta$ is not too different from $H(\rho)$. In fact, if the exact expression for F [Eq.(9)] is used, Eq. (26) agrees with the numerically computed (see next subsection) $\langle H(r,\theta)\rangle_\theta|_{r=0}$ to within a few percent.

We may use Eq. (27) to estimate roughly when the fast ion density produced by injection will be larger in the center of the plasma than at the outside. In view of its normalization, $\langle H(r,\theta)\rangle_\theta$ can be no larger than about unity at the outside of the plasma (see Fig. 4). Hence, if we are to deposit beam energy preferentially in the center, we may pick as a criterion that $H(\rho = 0) \gtrsim 1$. From Eq. (27) we obtain

$$\frac{a}{\lambda_o}\, e^{-\frac{a}{\lambda_o}\delta} \gtrsim \frac{r_B}{a} \sqrt{\frac{\delta R_c}{2R_o}} . \tag{28}$$

For injection into a reactor sized device, a/λ_o will be of order R_o/a while the right side of Eq. (28) will be of order $(r_B/a)\sqrt{a/R_o}$, which is quite small. Hence, Eq. (28) can be solved by iteration to yield the condition.

for depositing beam energy preferentially in the center of the plasma:

$$\frac{a}{\lambda_o} \lesssim \frac{1}{\delta} \ln \left\{ \frac{a}{r_B \delta} \sqrt{\frac{2R_o}{\delta R_c}} \ln \left[\frac{a}{r_B} \sqrt{\frac{2R_o}{\delta R_c}} \right] \right\} \sim 4 , \qquad (29)$$

for typical conditions.

4.3. COMPUTATIONAL RESULTS

The quantity of physical interest is the number of fast ions on a given flux surface, so we will consider the flux surface average of $H(r,\Theta)$, $\langle H(r,\Theta)\rangle_\Theta$. A set of plots of this quantity for ORMAK are shown in Figs. 4 and 5.

First, we notice that for $a/\lambda_o \lesssim 1$, the curves for counterinjection and coinjection are roughly equal. This is significant since each beam transfers a large amount of toroidal momentum to the plasma [16] and if the spatial density of fast particles from opposing beams is equal, this momentum input will be cancelled.

Labeled on each curve in Fig. 4 is the percent of the beam that is absorbed and contained in the plasma. More of the coinjected beam always is contained in the plasma since the counterinjected particles born in the outermost $2x_s$ of the plasma will hit the limiter. This effect becomes especially severe for $a/\lambda_o \gg 1$ since then a large fraction of the beam is deposited in this region even though the background plasma density is low there. This loss is also responsible for the discontinuity in the slope of the counterinjection curves.

Finally, as shown above it should be emphasized that the fast particle density will have its maximum in the center of the plasma even

with a/λ_o as large as 4, which is in contrast to commonly used estimates [12]. This surprising fact is essentially due to the exponential beam attenuation being compensated by the shrinkage of the drift surface area as the stagnation point is approached and hence the particles born in this region are spread less thinly than these born in the outer regions. This can be graphically seen by comparing Fig. 4 to Fig. 2 which does not have this geometric peaking effect included in it.

5. EFFECTS OF CHARGE EXCHANGE

In present tokamaks, a significant energy loss mechanism for the background plasma ions is charge exchange with neutrals [17]. Because of their greater speed, the injected fast ions have a slightly larger probability of charge exchanging before they can slow down and transfer their entire energy to the background plasma via Coulomb collisions.

We can assess the effect of charge exchange on the fast ion density profile if we 1) ignore any reionization of the resulting fast neutrals; 2) assume that the fast ions are confined to a flux surface; and 3) ignore the fast ion slowing down process. Then, we have

$$\frac{dn_f}{dt} = \frac{I_o}{2\pi^2 a^2 R_o e} \langle H(r,\Theta)\rangle_\Theta - n_f n_o \sigma_{cx} v_f \ , \tag{30}$$

where n_o is the cold neutral density profile and v_f is the speed of the fast ions. The solution of this equation is

$$n_f(r,t) = \frac{I_o \tau_{cx} \langle H(r,\Theta)\rangle_\Theta}{2\pi^2 a^2 R_o e} \left[1 - e^{-\frac{t}{\tau_{cx}}} \right] , \tag{31}$$

where

$$\tau_{cx}(r) = [n_o(r)\sigma_{cx} v_f]^{-1} \ . \tag{31}$$

Computer calculations [18] and measurements [17] show that the cold neutral profile rises monotonically with radius, has a value of from 2×10^8 to 2×10^9 particles/cm^3 at the center of the plasma in ORMAK, and is about 20 times larger near $r = a$. For $n_o = 10^9$ particles/cm^3, $\tau_{cx} \sim 8$ msec in ORMAK. Therefore, since $n_f(r,t) \sim \langle H(r,\theta)\rangle_\theta / n_o$, we see that n_f will become more peaked on axis than $\langle H(r,\theta)\rangle_\theta$ as time progresses (up to about $t \sim 2\tau_{cx}$). The extra peaking arises because the fast ion lifetime against charge exchange is longest on axis. Inclusion of the reionization of the fast neutrals before they leave the plasma, which has been ignored here, broadens the fast ion profile back towards the $\langle H(r,\theta)\rangle_\theta$ profiles in Fig. 4.

Accordingly, if the neutral density at $r = 0$ is high, the best strategy for injection is to place as many fast ions as possible in the center of the plasma independent of whether the maximum number of beam particles are absorbed by the plasma. As we saw in Section 3.1, the value of R_c for optimum beam absorption is $R_c = R_o - a/2$, for a parabolic density profile. However, the peak central value of the fast ion density can be maximized by injecting so that the beams are tangent to the torus at about the magnetic axis, $R_c \simeq R_o$. This effect is shown graphically in Fig. 5 where we plot $\langle H(r,\theta)\rangle_\theta$ versus r/a for $a/\lambda_o = 1/2$ in ORMAK with R_c as a parameter. As R_c is increased, the peak central value of fast ion density increases about 50% over the optimum absorption case. This point is further reinforced by Fig. 6 in which we plot the probability that a fast ion will be born within a given radius. In this case also, the net number of fast ions within a given radius will increase as R_c approaches R_o.

For experimental purposes, if the charge exchange problem is severe in a hydrogenic plasma, it may be reduced by using a helium plasma. In this case, as pointed out by J. R. McNally, Jr. [20], injection of fast H^o atoms can still be used to heat a He^{2+} plasma efficiently by taking advantage of the high quasi-resonance trapping cross section at the proper relative velocities. This is important since injecting helium atoms into a helium plasma is technologically difficult and would preclude the use of charge exchange ion temperature diagnostics.

Finally, we note that for the ORMAK standard parameters the slowing down time is $\sim$ 10 msec [19]. Thus, if $n_o(r=0)$ is less than about 5×10^8 cm^{-3} (as has been observed in ORMAK), most of the hot ions will be able to give their energy to the background plasma before charge exchanging, and this loss mechanism will be unimportant.

6. DISCUSSION AND CONCLUSIONS

In this paper we have dealt primarily with the details of injection geometry. In particular, we showed how to calculate and optimize the fast ion density profile arising from tangentially injected neutral beams.

We reemphasize the importance of the decreasing radius of the ion drift orbits as the stagnation point is approached. Because of the accompanying shrinkage in drift surface area, the fast ion density near the stagnation point can be higher than elsewhere even when the stagnation point is located up to 4 times λ_o away from the plasma edge. This has important implications for injection into a reactor since previous estimates limited the plasma radius to be less than only λ_o, or perhaps twice λ_o.

In order to compare tangential injection with the other possibility, perpendicular injection, we must consider the relevant geometrical distances. For parallel injection the distance from the plasma edge to the magnetic axis is just

$$d = \sqrt{(R_o+a)^2 - R_c^2} - \sqrt{R_o^2 - R_c^2} . \tag{32}$$

If $R_c = R_o - a/2$ (for optimum beam absorption), this distance is only about 1.5 a (in ORMAK), so that the path lengths for perpendicular injection (d = a) and parallel injection are not too different. On the other hand, if we inject so that $R_c = R_o$ (to peak the on axis fast ion density), $d = \sqrt{2R_o a + a^2} = 2.8$ a (in ORMAK), which is significantly larger than for perpendicular injection. However, the central density may still be peaked at the axis because the beam will be tangent to the axis at this point and hence dN_B/dR will be peaked there.

Since the profile of fast ions is strongly peaked at the center of the plasma in present day experiments where $a/\lambda_o \lesssim 1$, (see Fig. 4), we expect most heating as well as any deleterious effects due to injection to occur in this region. However, due to the peaking of the plasma density near the magnetic axis, McAlees [21] points out that even though the fast ion density is peaked there, the energy deposited per plasma particle and consequent plasma heating may not be peaked on axis.

From the calculated $\langle H(r,\Theta)\rangle_\Theta$ profiles, we can see that by adjusting the parameters of two opposing beams we can make the resulting two profiles almost equal on a flux surface-to-flux surface basis. This will allow approximate cancellation of any effect which depends upon the sign of $v_\parallel$ such as the momentum and current input to the plasma from the beams [16]. However, because the density peaks actually occur at the two

stagnation points and because the $H(\rho)$ profile is approximately constant for $\rho < r_B$, we see that if $r_B \lesssim x_s$, the equality of the fast ion densities from opposing beams can never occur except on a flux surface average basis.

Finally, we note that if charge exchange is an important loss mechanism for the fast ions, the best strategy for injection is to aim the injectors so that they are tangent near the magnetic axis in order to maximize the fast ion density and energy deposition there (cf. Fig. 5).

ACKNOWLEDGEMENTS

It is a pleasure to thank those who have helped us during the long gestation period of our injection studies. In particular, we mention J. T. Hogan, G. E. Guest, G. G. Kelley, T. C. Jernigan, S. Matsuda, D. G. McAlees, O. B. Morgan, D. J. Sigmar, and L. D. Stewart.

APPENDIX A

STANDARD ORMAK PARAMETERS

For the purposes of this work we define a "standard" plasma in the ORMAK experiment [17] with the following parameters:

Major radius: $R_o = 79.8$ cm

Minor (limiter) radius: $a = 23$ cm

Toroidal magnetic field: $B_T = 18$ kG

Toroidal plasma current: $I = 120$ kA

Inverse rotational transform: $q = rB_T/R_oB_p$; on axis, $q(0) = 2.2$

at limiter, $q(a) = 5$

Flat current time: 50 msec

Peak plasma density: $n = 3 \times 10^{13}/cm^3$

Peak electron temperature: $T_e(0) = 800$ eV

Peak ion temperature: $T_i(0) = 250$ eV

Neutral density on axis: $n_o(0) = 6 - 7 \times 10^8$

Average impurity content indicated by plasma resistance anomaly

relative to pure hydrogen: $\langle Z \rangle \leq 5$ where,

$$\langle Z \rangle = \frac{\sum_i \nu_{eZ_i}}{\nu_{eH}} = \frac{\sum_i n_i Z_i^2}{\sum_i n_i Z_i} = \frac{\sum_i n_i Z_i^2}{n_e}$$

in which $\sum_i$ is a sum over all ion species and the subscript H refers to hydrogen.

A single "standard" ORMAK neutral injector is similarly defined by the parameters [3]:

Neutral particles: H^o

Major radius at point of beam tangency: R_B adjustable from 65 to 75 cm

Beam divergence: 1.2° for half-width at half-maximum

Beam profile: essentially constant over a circular cross section of radius $r_B = 6$ cm at point of beam tangency

Beam components:

Energy (keV)	Power (kW)	Current
25	57	2.3
25/2	33	2.6
25/3	11	1.3
	101 kW	6.2 Amps Equivalent

REFERENCES

[1] G. G. Kelley, O. B. Morgan, L. D. Stewart, and W. L. Stirling, "Neutral-Beam-Injection Heating of Toroidal Plasmas for Fusion Research," Nuclear Fusion 12, 169 (1972).

[2] L. A. Artsimovich, "Tokamak Devices," Nuclear Fusion 12, 215 (1972).

[3] L. D. Stewart, R. C. Davis, J. T. Hogan, T. C. Jernigan, O. B. Morgan, and W. L. Stirling, "Neutral Beam Injection Heating of ORMAK," Paper E12, Third Intl. Symposium on Toroidal Plasma Confinement, Max-Planck-Institut für Plasma Physik, Garching (1973). See also Ref. [17].

[4] D. Aldcroft, J. Burcham, H. C. Cole, M. Cowlin, J. Sheffield, "The CLEO Tokamak Neutral Injection System," Nuclear Fusion 13, 393 (1973).

[5] K. Bol et al., "Adiabatic Compression of the Tokamak Discharge," Phys. Rev. Letters 29, 1495 (1972).

[6] R. Dei-Cas, S. deSacy, J. Druaux, D. Marty, and P. H. Rebut, "The Neutral Injection Heating Into the Fontenay-Aux-Roses Tokamak," Paper E9, Third Intl. Symposium on Toroidal Plasma Confinement, Max-Planck-Institut für Plasma Physik, Garching (1973).

[7] T. Ohkawa, "New Methods of Driving Plasma Current in Fusion Devices, Nuclear Fusion 10, 185 (1970).

[8] L. D. Stewart et al., "Neutral Beam Injection Heating of Tokamaks, Paper E8, Third Intl. Symposium on Toroidal Plasma Confinement, Max-Planck-Institut für Plasma Physik, Garching (1973).

[9] R. J. Bickerton, J. W. Connor, and J. B. Taylor, "Diffusion Driven Plasma Currents and Bootstrap Tokamak," Nature, Phys. Sci. 229, 110 (1971).

[10] D. J. Sigmar, "Bootstrap Current in Tokamaks with Neutral Injection," Nuclear Fusion 13, 17 (1973).

[11] A. C. Riviere, "Penetration of Fast Hydrogen Atoms Into a Fusion Reactor Plasma," Nuclear Fusion 11, 363 (1971).

[12] D. R. Sweetman, "Ignition Condition in Tokamak Experiments and Role of Neutral Injection Heating," Nuclear Fusion 13, 157 (1973).

[13] T. G. Northrop, The Adiabatic Motion of Charged Particles John Wiley, New York (1963).

[14] T. H. Stix, "Heating of Toroidal Plasmas by Neutral Injection," Plasma Physics 14, 367 (1972).

[15] J. D. Callen, J. F. Clarke, and J. A. Rome, "Neutral Beam Injection Into a Tokamak II: Evolution of Neutral Injected Particles," (to be published).

[16] J. D. Callen, J. F. Clarke, and J. A. Rome, "Theory of Neutral Beam Injection Into a Tokamak," Paper E14, Third Intl. Symposium on Toroidal Plasma Confinement, Max-Planck-Institut für Plasma Physik, Garching (1973).

[17] G. G. Kelley et al., "Status of the ORMAK Experiment," Paper B3-1, Third Intl. Symposium on Toroidal Plasma Confinement, Max-Planck-Institut für Plasma Physik, Garching (1973).

[18] J. T. Hogan, J. F. Clarke, and H. Postma, "Neutrals in ORMAK," in ORNL Thermonuclear Division Annual Progress Report for Period Ending December 31, 1970, p. 56.

[19] J. G. Cordey and M. J. Houghton, "Problems Associated with the Injection of a High-Energy Neutral Beam Into a Plasma," Nuclear Fusion 13, 125 (1973).

[20] J. R. McNally, Jr., "Neutral Injection Heating of Tokamaks," submitted to Nuclear Fusion.

[21] D. G. McAlees, private communication.

FIGURE CAPTIONS

Fig. 1. Geometry of neutral beam injection into a torus: (a) cross sectional view showing a diffuse neutral beam at its point of tangency; (b) top view showing a pencil beam.

Fig. 2. The production rate of the fast ions along the beam path. Contributions from both the ingoing ($s < 0$) and outgoing ($s > 0$) parts of the neutral beam path have been added.

Fig. 3. The time rate of change of the fast ion density as a function of the distance from the stagnation point for a pencil beam in the equatorial plane. $R_B = 68.5$ cm, $\lambda_o = 46$ cm, and hence $a/\lambda_o = 1/2$ in ORMAK.

Fig. 4. Spatial shape factor for the fast ion density distribution, $\langle H(r,\theta)\rangle_\theta$, for various values of a/λ_o. The percentage of the beam ions that are absorbed by, and stay in the plasma is labeled on each curve. $R_c = 68.5$ cm, $x_s = 2.8$ cm in ORMAK.

Fig. 5. Spatial shape factor for the fast ion density distribution, $\langle H(r,\theta)\rangle_\theta$, for various values of R_c. $a/\lambda_o = 1/2$, $x_s = 2.8$ cm in ORMAK.

Fig. 6. The fraction of fast ions absorbed within a given radius for various values of R_c. $a/\lambda_o = 1/2$, $x_s = 2.8$ cm in ORMAK.

TABLE I

COLLISION CROSS SECTIONS AND MEAN FREE PATHS FOR THE

THREE ENERGY COMPONENTS OF THE ORMAK INJECTOR

E(keV)	σ_{cx}, Charge Exchange ($\mathring{A}^2$)	σ_{ei}, Electron Ionization ($\mathring{A}^2$)	σ_{pi}, Proton Ionization ($\mathring{A}^2$)	σ_T Total ($\mathring{A}^2$)	Fraction by Charge Exchange	Mean Free Path (cm) $\lambda_o = 1/n\sigma_T$
25	5.0	1.0	1.3	7.3	0.68	46
25/2	7.5	1.5	1.0	10.0	0.75	33
25/3	9.5	2.0	0.5	12.0	0.79	28

ORNL-DWG 73-7356

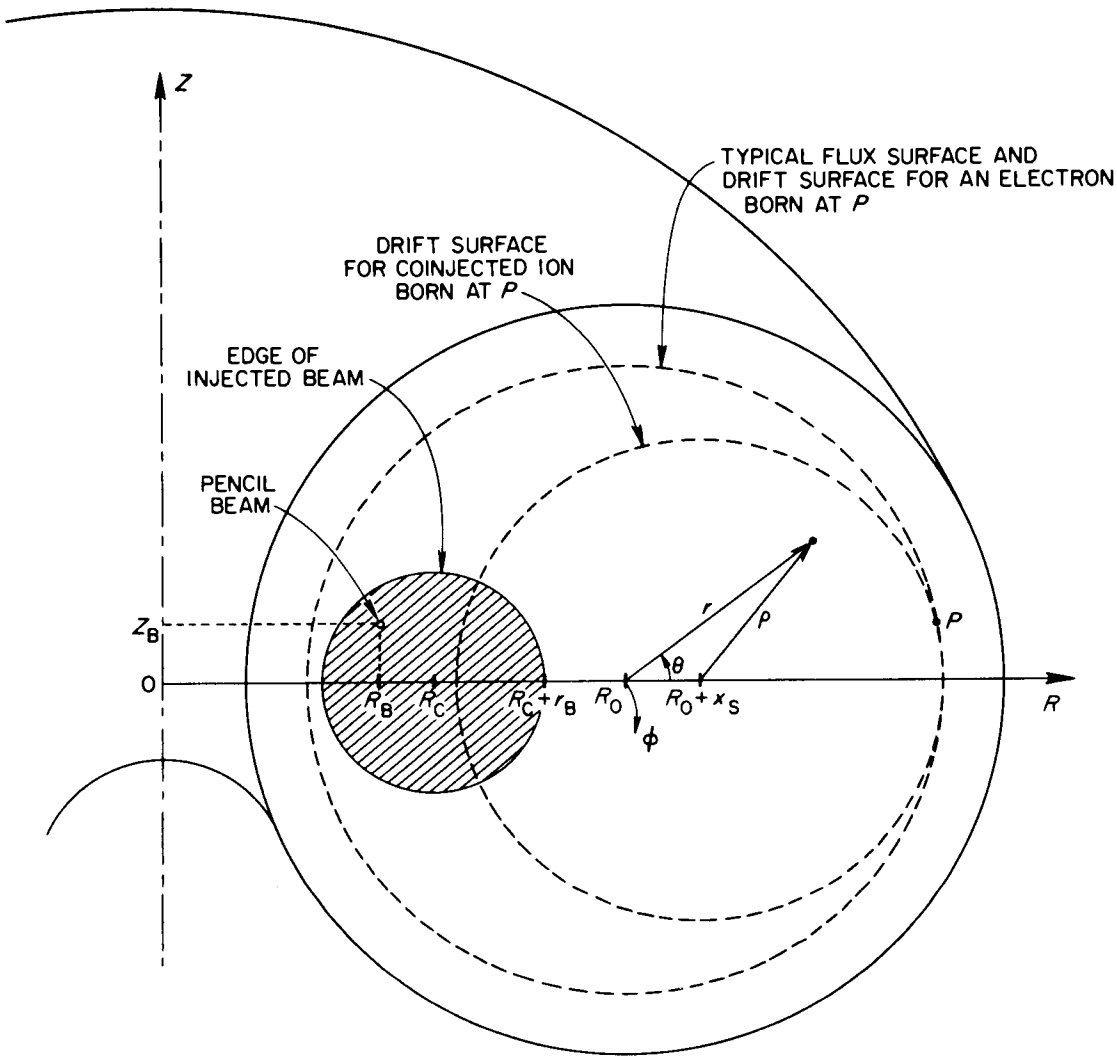

Figure 1A

ORNL-DWG 73-7355

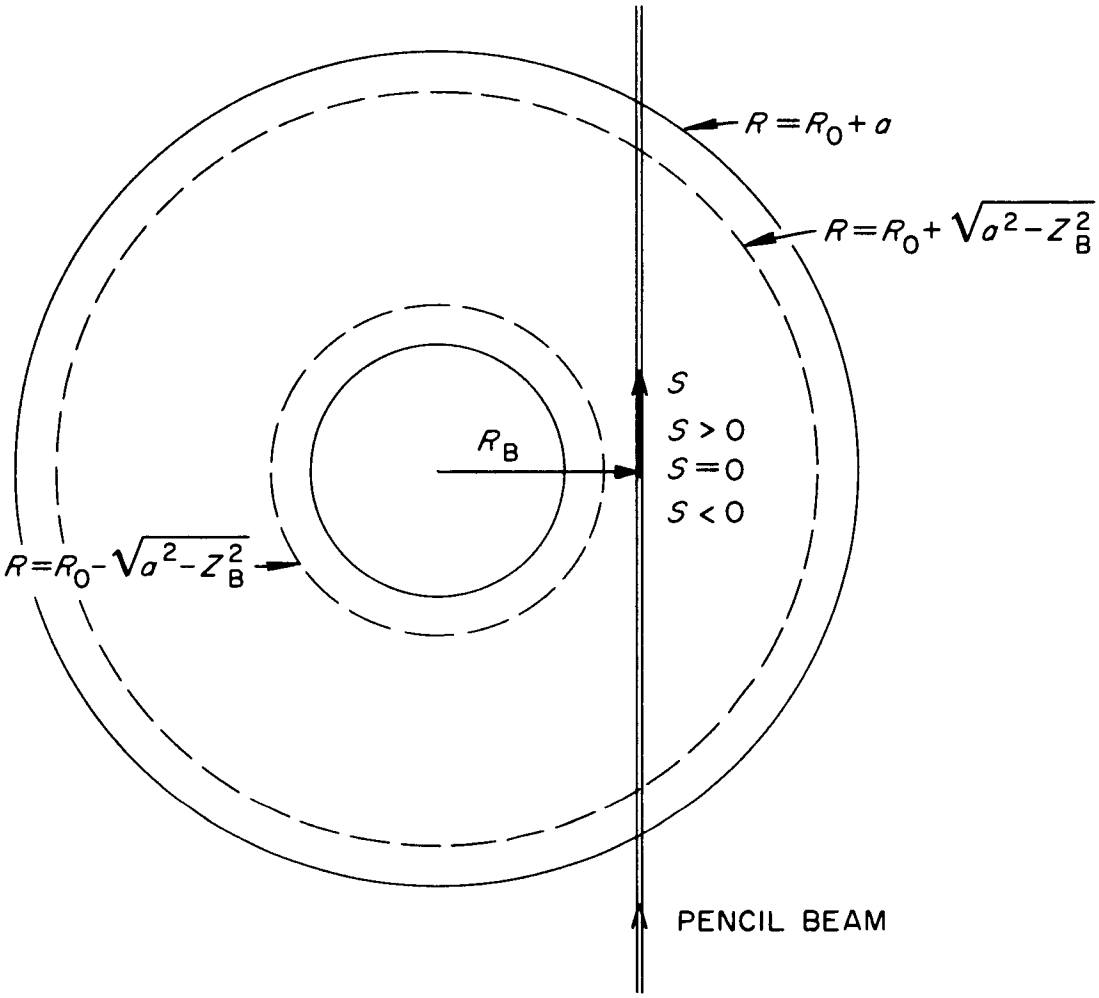

Figure 13

ORNL-DWG 73-7354

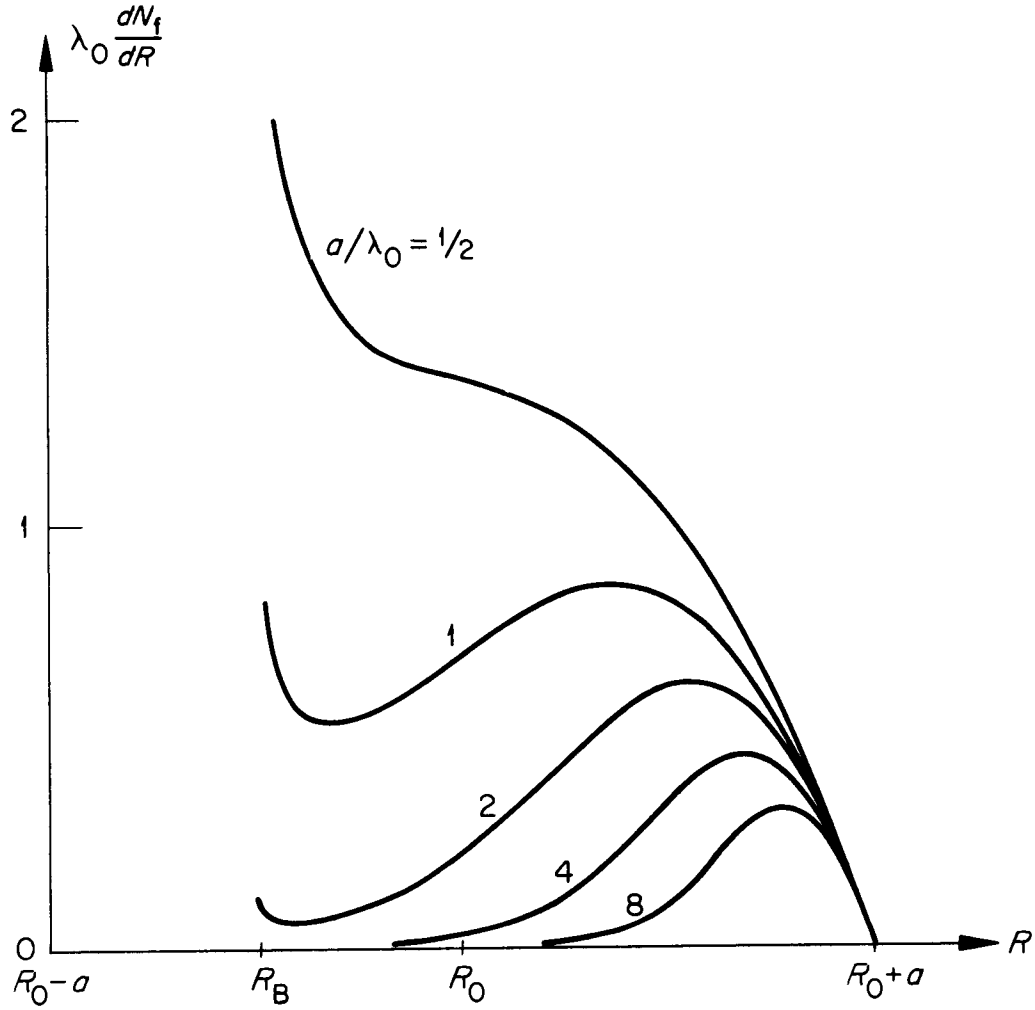

Figure 2

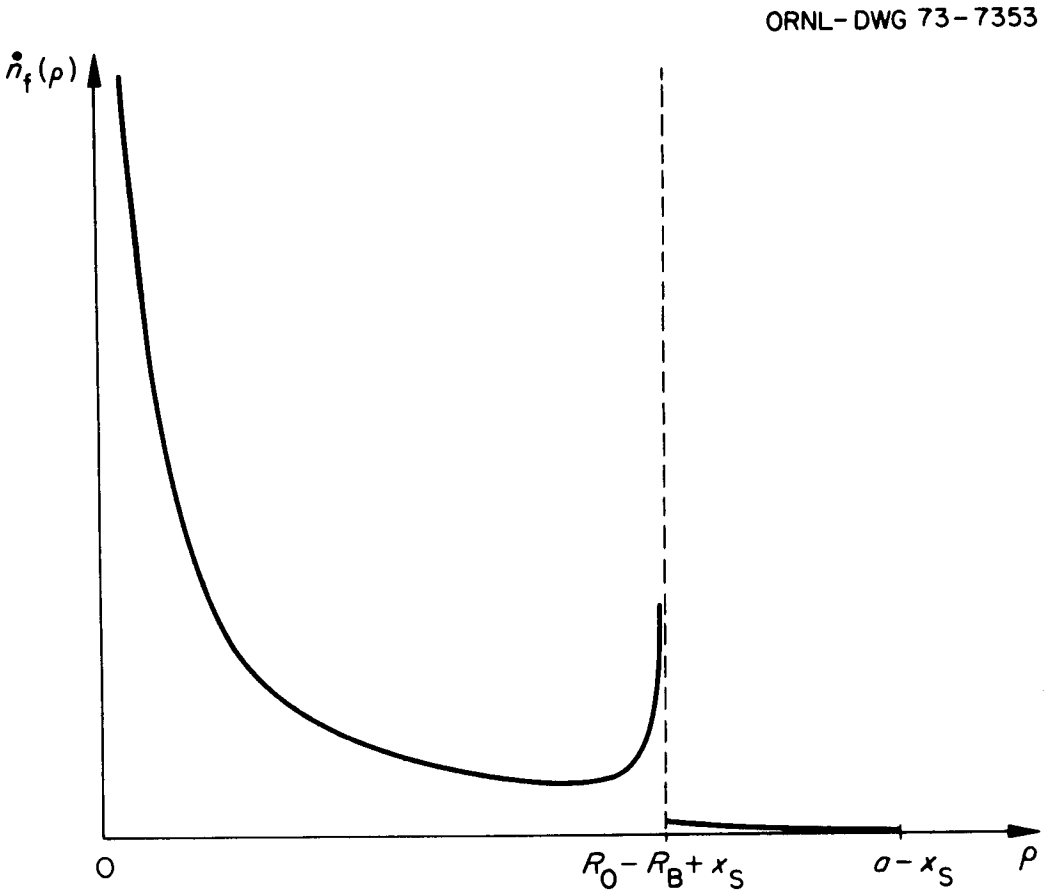

Figure 3

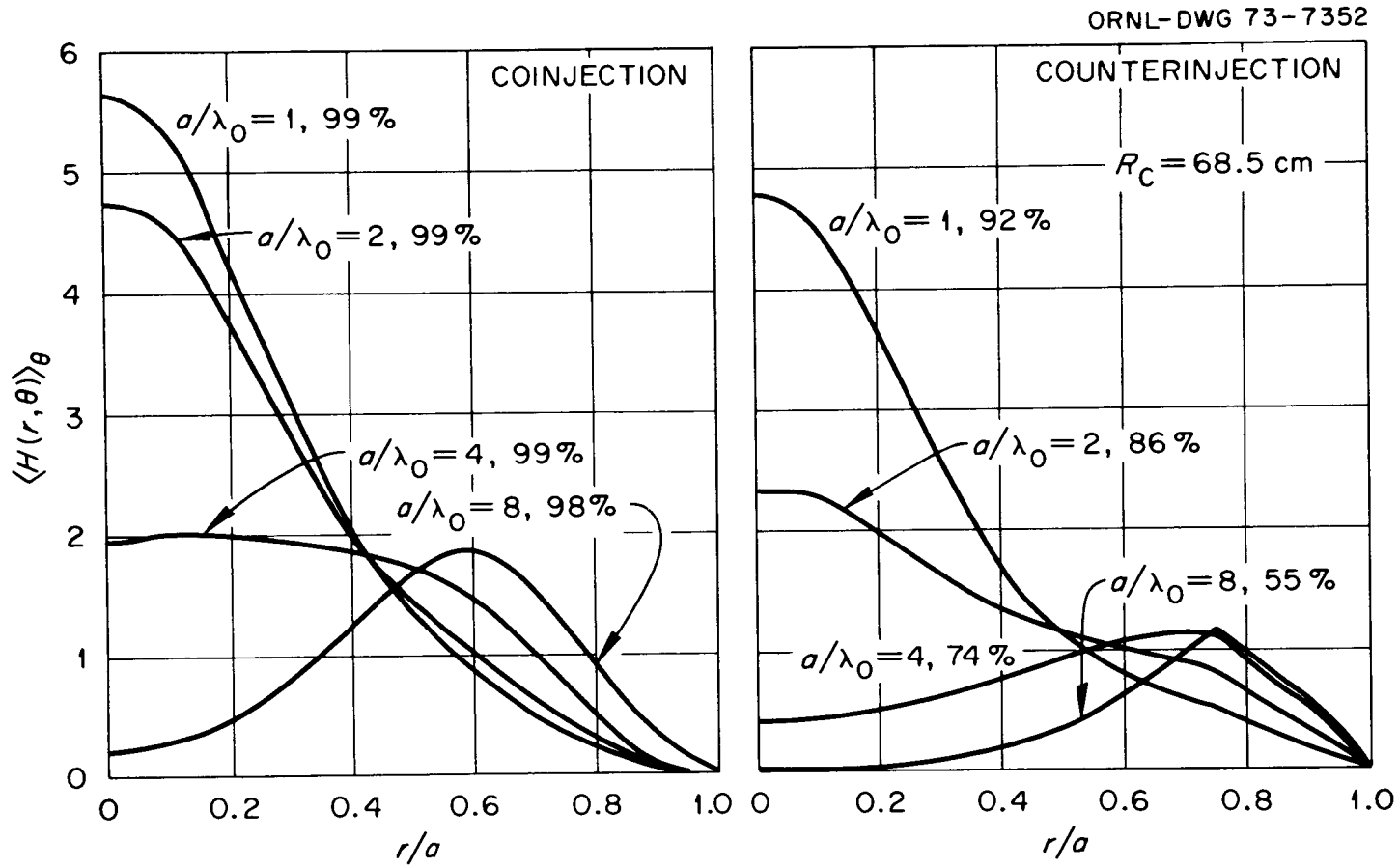
ORNL-DWG 73-7352
COINJECTION
COUNTERINJECTION
$a/\lambda_0 = 1$, 99 %
$a/\lambda_0 = 2$, 99 %
$a/\lambda_0 = 4$, 99 %
$a/\lambda_0 = 8$, 98 %
$R_C = 68.5$ cm
$a/\lambda_0 = 1$, 92 %
$a/\lambda_0 = 2$, 86 %
$a/\lambda_0 = 8$, 55 %
$a/\lambda_0 = 4$, 74 %
$\langle H(r,\theta)\rangle_\theta$
r/a
0
1
2
3
4
5
6
0.2
0.4
0.6
0.8
1.0

Figure 4

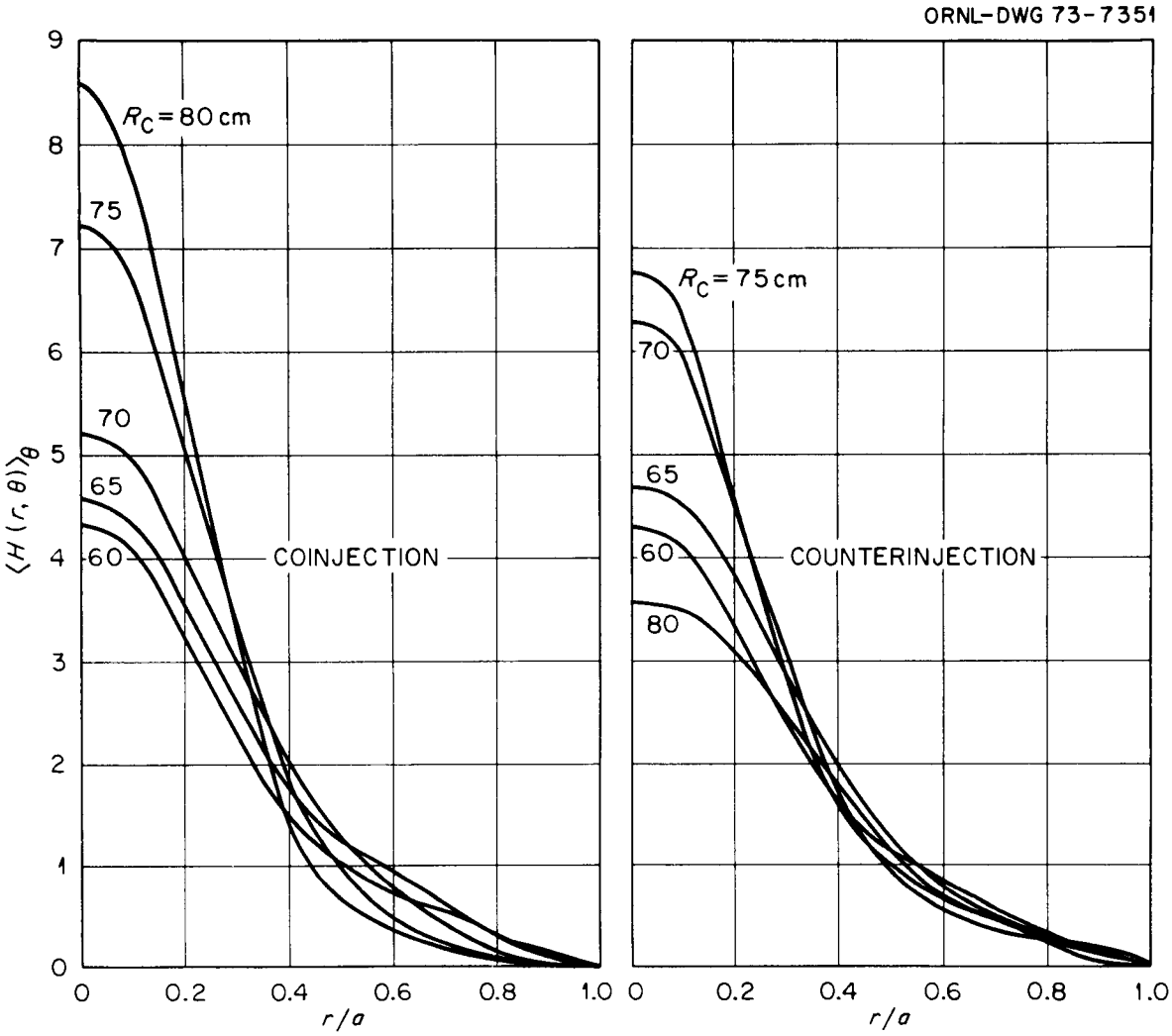
ORNL-DWG 73-7351
$R_C = 80$ cm
75
70
65
60
COINJECTION
$R_C = 75$ cm
70
65
60
80
COUNTERINJECTION
$\langle H(r,\theta)\rangle_\theta$
0
1
2
3
4
5
6
7
8
9
0
0.2
0.4
0.6
0.8
1.0
r/a

Figure 5

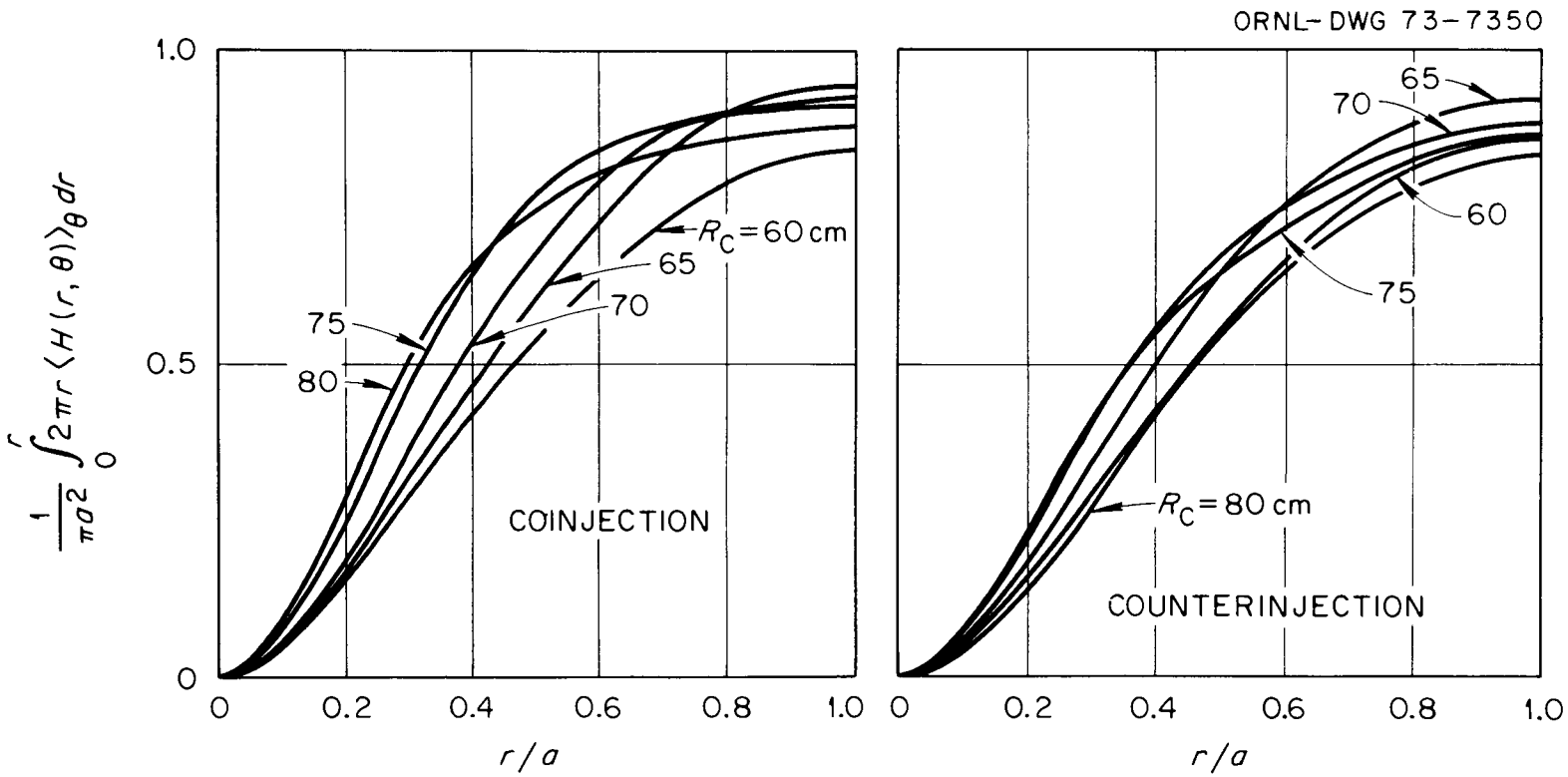
ORNL-DWG 73-7350
$\frac{1}{\pi a^2}\int_0^r 2\pi r \langle H(r,\theta)\rangle_\theta dr$
1.0
0.5
0
0
0.2
0.4
0.6
0.8
1.0
r/a
R_C = 60 cm
65
70
75
80
COINJECTION
R_C = 80 cm
60
65
70
75
COUNTERINJECTION

Figure 6